Proceedings of FEDSM'98
1998 ASME Fluids Engineering Division Summer Meeting
June 21-25, 1998, Washington, DC

FEDSM98-4945

EFFECTS OF EXTERNAL DISTURBANCES ON THE MOMENTUM TRANSPORT IN CASCADE TRANSITIONAL BOUNDARY LAYER FLOWS

LUIS R. ROJAS-SOLORZANO.
DEPARTAMENTO DE CONVERSION Y
TRANSPORTE DE ENERGIA
UNIVERSIDAD SIMON BOLIVAR
CARACAS, VENEZUELA, A.P. 89000
e-mail: rrojas@usb.ve

ABSTRACT

The effects on the boundary layer receptivity in airfoil cascade flow caused by superposed disturbances are studied using an energetic approach. The separated terms in the Fluctuating Kinetic Energy (FKE) budget are calculated. Monotonic time-harmonic disturbances are superposed to the inflow stream using forcing frequencies close to and far from the natural frequency of fluctuation ω_n found within the unsteady (supercritical) basic flow. For supercritical regimes, the receptivity is evaluated around the boundary layer separation point, where Tollmien-Schlichting (T-S) waves are *naturally* generated. For subcritical regimes, the receptivity is explored all over the suction-side of the airfoil since separation does not occur. Within subcritical flows, the superposed perturbation is seen to trigger the generation of T-S-like waves downstream the minimum pressure point only when the forcing frequency is close to ω_n. Within supercritical flows, when the forcing frequency matches ω_n, the FKE budget reflects the energetic interaction between the perturbation and the already existent boundary layer T-S waves.

INTRODUCTION

Laminar to turbulent flow transition is in many cases a progressive and evolutive phenomenon which starts with the perturbation of a unstable mean flow originally in equilibrium and the subsequent development of flow instabilities. The generation of these primary instabilities is denominated the receptivity phenomenon. These initial instabilities are named Tollmien-Schlichting (T-S) waves and are typically two-dimensional with exponential convective evolution within linear bounds. The fluid dynamic properties determine whether these waves will grow or die and, in the first case will also determine the subsequent three-dimensional and non-linear evolution of the transitional waves that precede turbulence. This pattern of transition is denominated natural transition.

This study explores the effects caused by monotonic time-harmonic perturbations on the boundary layer receptivity in both weakly transitional flow regimes and within steady state flows. The study of the receptivity is here undertaken by computing the momentum exchange between the mean flow and the fluctuations.

Previous studies of the boundary layer receptivity have succeeded in demonstrating that receptivity occurs in regions where the mean flow suffers rapid changes in the streamwise direction (e.g., Dovgal et al., 1986; Goldstein 1985a, 1985b). These changes might be attributed to geometric irregularities or to dynamical adjustments in the flow stream. In particular, Rojas & Amon (1997) demonstrated that the natural generation of T-S waves is associated to the boundary layer separation occurring on the airfoil suction-side above the critical Re=375. We also demonstrated the apparition of short

wavelength instabilities within steady boundary layers when perturbed with frequencies close to the natural frequency. The previous investigation was based in observation of the velocity and pressure fields and, although this allowed us to visualize and measure the receptivity phenomenon, still physical explanation of the receptivity is necessary. It seemed to us that receptivity might be better understood through and energetic approach which will link the different mechanisms governing the momentum exchange between the mean flow and the instabilities.

Thus, here we compute the Fluctuating Kinetic Energy (FKE) budget within a supercritical basic oscillatory flow and within perturbed flows.

The FKE budget is traditionally used as an efficient tool to characterize the intensity and nature of the momentum exchange between the mean flow and the fluctuations.

The first part of the paper introduces the FKE budget and briefly explains the meaning of its components. In the second part, the geometry, governing equations and the numerical approach are described. The third part includes a review of previous results. The final section presents the results and conclusions.

NOMENCLATURE

c	= chord length of airfoil [ft]
d_n	= distance from wall in normal direction [ft]
h	= pitch [ft]
p*	= pressure [lbm/ft-s^2]
p	= non-dimensional pressure ($p^*/\rho.U_\infty^2$)
Re	= Reynolds number ($U_\infty.c/\nu$)
Sp*	= magnitude of velocity vector (speed) [ft/s]
Sp*'	= oscillatory component of the speed [ft/s]
Sp'	= non-dimensional Sp*' (Sp*'/U_∞)
t*	= time [s]
t	= non-dimensional time ($t^*.U_\infty/c$)
u*,v*	= x- and y-velocity [ft/s]
u*',v*'	= fluctuating x-and y-velocity [ft/s]
u,v	= u*/ U_∞ and v/ U_∞
u',v'	= u*'/ U_∞ and v*'/ U_∞
U_∞	= inlet average velocity [ft/s]
$\vec{u}^*$	= velocity vector [ft/s]
$\vec{u}$	= $\vec{u}/U_\infty$
x*	= x-axis distance [ft]
y*	= y-axis distance [ft]
x	= x*/c
y	= y*/c

FKE Budget

The kinetic energy budget for the fluctuating components of the velocity and pressure (1) results from the time-averaged momentum and mass conservation equations, departing from the Reynolds decomposition of the velocity vector and the pressure (Hinze, 1987). The equation (1) represents the conservation of FKE in the elementary control volume depicted in Fig. 1.

The equation (1) essentially states that within an elementary control volume the balance among the diffusive transport of FKE by the fluctuations, the work of the fluctuations to diffuse through the viscous field, the production and dissipation must equal the time rate of increase of FKE and the convective diffusion of FKE by the mean flow. This equation is expressed as :

$$\underbrace{\frac{D}{Dt}\overline{q'}}_{T1,T2} = \underbrace{-\frac{\partial}{\partial x_i}\overline{u'_i\left(p'+q'\right)}}_{T3} \underbrace{-\overline{u'_i u'_j}\frac{\partial U_i}{\partial x_j}}_{T4} + \underbrace{\frac{1}{\mathrm{Re}}\frac{\partial}{\partial x_i}\overline{u'_j\left(\frac{\partial u'_i}{\partial x_j}+\frac{\partial u'_j}{\partial x_i}\right)}}_{T5} \underbrace{-\frac{1}{\mathrm{Re}}\overline{\left(\frac{\partial u'_i}{\partial x_j}+\frac{\partial u'_j}{\partial x_i}\right)\frac{\partial u'_j}{\partial x_i}}}_{T6}$$

$$\Downarrow$$

$$T1 = \frac{\partial}{\partial t}\left(\frac{u'_i u'_i}{2}\right)$$

$$T2 = \frac{\partial}{\partial x_i}\left(U_i \frac{u'_j u'_j}{2}\right) \qquad (1)$$

where,

q'	: fluctuating kinetic energy FKE=(u_1'^{2}+u_2'^{2})/2
$-u'_iu'_j$	: fluctuating (Reynolds) shear stress
U_i	: time-averaged velocity
T1	: time rate of increase of FKE
T2	: convective diffusion of FKE by the mean flow
T3	: work of the fluctuating dynamic pressure
T4	: production of FKE
T5	: work of the viscous shear stresses of the fluctuations
T6	: viscous dissipation of FKE

Terms T1-T6 are non-dimensionalized by c/U_∞^3.

Although the FKE budget is traditionally used in the study of turbulent flows, it has proven to be useful in the investigation of different energy transfer mechanisms between the mean and the fluctuating flow in weakly transitional regimes (e.g., Majumdar & Amon, 1997).

MODELING AND APPROACH

MATHEMATICAL MODEL

The geometry under consideration, depicted in Fig. 2, corresponds to the midspan blade-to-blade surface of an experimental stator row (Dring, Blair, Joslyn, Power & Verdon, 1988).

The governing equations are the incompressible two-dimensional Navier-Stokes and conservation of mass equations:

$$\frac{\partial \vec{u}}{\partial t} + \vec{u}.\nabla\vec{u} = -\nabla p + \frac{1}{\mathrm{Re}}\nabla^2\vec{u} \quad \text{in } \partial D \qquad (2)$$

$$\nabla . \vec{u} = 0 \quad \text{in } \partial D \qquad (3)$$

where, ∂D is the computational domain and the non-dimensionalization is given in the nomenclature section. The mathematical problem is subject to the following boundary conditions:

a) inflow

a.1) basic flow

$$u_{H-A} = 1 \; ; \; v_{H-A} = 0$$

a.2) perturbed flow

$$u_{H-A} = 1 + u' \; ; \; v_{H-A} = 0$$

where, $u' = \varepsilon . \sin(\omega_d . t)$

b) outflow

$$\left.\frac{\partial u}{\partial x}\right|_{(D-E)} = 0$$

$$\left.\frac{\partial v}{\partial x} + \frac{\partial u}{\partial y}\right|_{(D-E)} = 0$$

c) blade wall

$$u_{B-C} = u_{G-F} = 0$$

d) meridional bounds

$$u_{A-B} = u_{G-H} \; ; \; u_{C-D} = u_{E-F}$$

$$v_{A-B} = v_{G-H} \; ; \; v_{C-D} = v_{E-F}$$

The reference corners A through H are depicted in Fig. 2.

NUMERICAL APPROACH

DNS is used to solve the discretized governing equations. The spatial discretization of the domain is conducted using the spectral element technique (Patera, 1984; Korczag & Patera, 1986; Amon, 1993). The complete solution of the Navier-Stokes equations involves first treating the wave-like equation for the non-linear convective terms explicitly, and then solving the resultant Stokes problem at each time-step by the Uzawa iterative procedure (Rønquist, 1988).

Details of the formulation and the methodology may be encountered in Rojas & Amon (1995).

The spectral mesh with 784 elements along with the 25 collocation points for three contiguous blades is depicted in Figure 3.

BASIC OR UNPERTURBED FLOWS

The unperturbed or basic flows considered in this study cover a Re range that allowed us to study both a stable steady state regime (Re=231) and a self-sustained fluctuating regime (Re=1000). Iso-pressure lines are presented in Fig. 4 for the mean flow at Re=1000. This figure (qualitatively the same for the slower regime, Re=231) shows the suction-side under favorable pressure gradient only over the first 50% of the airfoil axial length, while adverse pressure gradient acts elsewhere towards the trailing edge.

The flow for Re=231 is time-independent, whereas boundary layer separation downstream the minimum pressure point along with spatial and temporal fluctuations are noticed for Re=1000. Spatial evolution of fluctuations at three different times close to the wall within the suction-side boundary layer in Fig. 5, shows the generation and evolution of T-S waves within the basic flow at Re=1000. This phenomenon is better observed in Fig. 6. This figure shows a carpet plot of the fluctuations within the whole domain, and within the suction-side boundary layer.

The instability depicts a long wavelength at the airfoil leading edge and thereafter convects downstream driven by the mean flow. Downstream the minimum pressure point, the instability suffers a wavelength-modulation process that terminates at the separation point where the original instability finally becomes a transitional short-wavelength instability, i.e., a T-S wave.

The calculation of the FKE budget is performed thoroughly within the entire domain. However, some scatter in the pressure term (T3), product of the large gradients and the discontinuity in the derivatives across the boundary of contiguous mesh elements suggested the calculation of the pressure term as the balance of the kinetic equation. This step required that T1=0. This condition for T1, is consistent with the fact that although we are dealing with unsteady flows, in the time-average the flow is stable and in equilibrium with no punctual gain or loss of FKE.

Figure 7 shows the FKE budget for Re=1000 at five different perpendicular stations: mid-way beyond the leading edge (L_3), slightly downstream the minimum pressure point (L_5), just at the separation point (L_6), in the middle of the separated bubble (L_7) and close to the trailing edge (L_8).

The FKE budgets are presented as a function of the normal distance to the wall d_n, non-dimensionalized by the local boundary layer thickness δ. At the entrance (L_3), moderate dissipation of energy T6 over the wall is accompanied by a favorable fluctuating pressure term T3 which provides FKE uniformly across the section to sustain the convection T2 of the long wavelength instability generated at the leading edge. The production term T4, as expected under favorable pressure gradient, is almost negligible within the lower half of the boundary layer, and negative within the upper half. A negative T4 indicates that the mean flow withdraws energy from the instability and promotes its stabilization. Between the minimum pressure point and the separation point, at L_5, the FKE budget describes the energy transport during the wavelength modulation process that gives rise to the receptivity phenomenon, i.e., the generation of T-S waves.

While the fluctuating pressure field T3 offers resistance to the convection of the instability within the lower half of the boundary layer, the production is intensive around the inflection point and assists the wavelength modulation. The largest production of FKE around the inflection point reflects the highest level of shear stress and vorticity associated to the inflection point in the mean flow. Since the shear stress and the vorticity are measures of the level of deformation and rotational velocity of the fluid particles, respectively, it is expected that the largest deformation of the mean flow causes the largest amount of work by the mean flow against the fluctuating shear stresses, i.e., T4. Within the boundary layer upper half, the production is negligible, and the work by the fluctuating pressure, T3, becomes the driving force that sustains the instability convection above the mean flow, T2.

PERTURBED FLOWS

In a previous measure of the local receptivity (Rojas & Amon, 1997), it was found that, when the flow is perturbed with the appropriate frequency, either existent T-S waves in non-steady basic flows (Re=1000) were enhanced, or T-S waves were artificially generated in steady basic flows (Re=231). The later was also confirmed by observation of short wavelength instabilities developing downstream the minimum pressure point within the boundary layer. The visualization of the boundary layer receptivity and stability is depicted in Fig. 8 with a carpet plot of the fluctuating speed Sp' for Re=1000 at the moment when the forced perturbation vanishes.

The plots contrast the appearance of the Sp' field within the basic flow and for two perturbed cases. The clear enhancement in the T-S waves is noticed for the case with ω_d=26.4, while the instability amplitude is not affected by the perturbation with ω_d=88.0. The flow behavior for the case with ω_d=26.4 demonstrates the non-linear interaction between the perturbation and the natural instabilities giving rise to a resonance phenomenon that enhances the amplitude of the existent T-S waves.

Results of the FKE budget at stations L4, L5 and L7 are presented in Fig. 9a for Re=231 y Fig. 9b for Re=1000.

For Re=231, at station L_4 the flow field is under favorable pressure gradient and the transport of FKE by the fluctuating pressure is uniformly enhanced by the superposed perturbation above 30% of the boundary layer thickness, independently of the perturbation frequency. Within the lower 30% of the boundary layer thickness, the development of a Stokes-like layer is noticed. The uniform and positive distribution of T3 within the upper region of the boundary layer provides the necessary energy to convect the Stokes-like wave along with the mean flow (T2). The non-uniform and frequency-dependent T3, within the Stokes layer, sustains the convection of the Stokes waves close to the wall where the viscous demands (T5) are more significant. At station L_5, the boundary layer is under adverse pressure gradient and the Stokes layer is still noticeable. Above the Stokes layer, the distributions of T2 and T3 are reversed compared to the precedent stations though, do not show differences between the two cases.

Further downstream under APG, at station L_7, for the case with ω_d=26.4, the boundary layer receptivity is evident. The receptivity occurs as the fluctuating pressure field (T3) offers an enhanced resistance to the evolution of the Stokes wave. This resistance assists the wavelength modulation that is taking place and gives rise to the generation of the T-S wave under a preferential perturbation frequency (ω_d=26.4). The wavelength modulation is supported with FKE supplied by the mean flow convection (T2). Underneath the Stokes layer, the FKE budget does show the non-uniform frequency-related distribution of T3 observed in the previous stations.

For the supercritical regime (Re=1000), the FKE budgets at stations L_2 and L_5 are in excellent agreement with the FKE budgets from the perturbed subcritical flow, confirming that up to station L_5 the perturbation has just superposed to the basic flow without nonlinear interaction.

In the region of adverse pressure gradient, at station L_7, the FKE transport is remarkably different to what happens to the subcritical flow (Re=231). Within the bubble, the FKE budgets reflect the energetic interaction between the T-S waves and the induced Stokes waves according to the perturbation frequency. The case for the larger frequency (ω_d=88.0) not only shows lower levels of enhancement in the energy transport mechanisms than for the case with frequency approximately matching the natural frequency (ω_d=26.4), but a different qualitative distribution. For example, at station L_7 the flow perturbed with ω_d=88.0 depicts negative levels of production (T4) indicating that the fluctuations attributed to the induced Stokes waves and the evolving T-S waves release energy to the mean flow. At the same time, that energy is provided to the waves by a favorable fluctuating pressure gradient, thus balancing the energy transfer. At the same station, the flow perturbed with ω_d=26.4 shows a marked interaction between the Stokes wave and the T-S waves traveling within the bubble, as the FKE production is promoted within the lower half of the boundary layer and inhibited within the upper half. The fluctuating pressure gradient (T3) plays a fundamental role in the convection of the T-S waves within the upper half of the boundary layer.

CONCLUDING REMARKS

The boundary layer receptivity and evolution of Tollmien-Schlichting (T-S) waves within an experimental airfoil cascade are studied through the mechanisms of momentum exchange and energy transformation between the mean flow and the fluctuations for basic flows and for flows with superposed

time-harmonic disturbances. The study covers the Re number (Re) range of 231-1000.

For unsteady basic flows at Re=1000, the initiation of the instability wavelength modulation process, marked by the minimum pressure point, is accompanied by the production of FKE predominantly around the mean velocity inflection point. Above and underneath the inflection point, the production decays gradually towards the boundary layer edges. The production of FKE mainly accounts for the energy demanded to convect the instability against an adverse fluctuating pressure gradient while the wavelength contraction is taking place. Above the inflection point, the fluctuating pressure gradient favors the convection of instabilities out of the boundary layer. The evolution of T-S waves within the separated bubble is characterized by a transverse asymmetric production of FKE; positive within the lower half of the boundary layer and negative within the upper half. The positive production reaches its maximum around the inflection point. Within the upper half of the boundary layer, the T-S wave convection is intensified by the action of the fluctuating pressure field.

For perturbed flows, the time-harmonic disturbance superposed to the originally basic flow has a well defined global incidence on the energy transport characteristics. Within the favorable pressure gradient region, the superposed disturbance generates a sublayer, within the lower half of the boundary layer thickness, very close to the wall. Within the sublayer, the unsteady pressure field favors the convection of both the generated Stokes wave and the leading edge-associated long wavelength instability. Above the sublayer, the unsteady pressure contributes FKE with less but uniform intensity to support mainly the instability convection. Further downstream, under adverse pressure gradient, the role of the sublayer becomes less important.

In the study of the effects of the forced disturbance on the boundary layer receptivity and stability, we explain separately the perturbed flow behavior for otherwise steady flow regimes (Re=231) and for self-fluctuating flow regimes (Re=1000).

For Re=231, under adverse pressure gradient region, the boundary layer is essentially indifferent to the perturbations within its lower half. However, within the upper half, T-S waves are generated for the case with perturbation matching the natural frequency. The T-S wave generation, i.e., the boundary layer receptivity phenomenon, is characterized by the retarding action of an adverse unsteady pressure field assisting the wavelength modulation of the Stokes wave. Once the T-S wave is generated, its convection is strongly promoted by a favorable unsteady pressure field.

For Re=1000, the receptivity gives rise to the naturally-generated T-S waves and is unaffected by the disturbances. However, the stability of the boundary layer, i.e., the evolution of existent T-S waves, is dramatically affected. For the flow perturbed with a disturbance matching the natural frequency, the resonance found in the flow field visualization is also illustrated by the FKE budget. In such a case, it is noticed an enhancement in the production of FKE within the boundary layer lower half and a large amount of FKE supplied by the unsteady pressure field to assist the T-S wave convection within the upper half.

REFERENCES

Amon, C.H., 1993, "Spectral Element-Fourier Method for Transitional Flows in Complex Geometries," AIAA Journal, Vol. 31, No. 1, pp. 42-48.

Dovgal, A.V., Kozlov, V.V., and Simonov, O.A., 1986, "Experiments on Hydrodynamic Instability of Boundary Layers with Separation," Boundary-Layer Separation, IUTAM Symposium, F. T. Smith, and S. N. Brown, eds., Springer-Verlag, Berlin, pp. 109-130.

Dring, R.P., Blair, M.F., Joslyn, H.D., Power, G.D., and Verdon, J.M., 1988, "The Effects of Inlet Turbulence and Rotor/Stator Interactions on the Aerodynamics and Heat Transfer of a Large-Scale Rotating Turbine Model, I-Final Report," NASA Contractor Report 4079.

Goldstein, M.E., 1985a, "Scattering of Acoustic Waves into Tollmien-Schlichting Waves by Small Streamwise Variations in Surface Geometry," Journal of Fluid Mechanics, Vol. 154, pp. 509-529.

Goldstein, M.E., 1985b, "The Generation of Tollmien-Schlichting Waves by Long Wavelength Free-Stream Disturbances," Stability of Time Dependent and Spatially Varying Flows, D.L. Dwoyer and M.Y. Hussaini, eds., Springer-Verlag, New York, pp. 58-81.

Hinze, J.O., 1987, "Turbulence," McGraw-Hill Publishing Company, 2nd ed., New York.

Korczak, K.Z., and Patera, A.T., 1986, "An Isoparametric Spectral Element Method for Solution of the Navier-Stokes Equations in Complex Geometry," Journal of Computational Physics, Vol. 62, pp.361-382.

Majumdar, D., and Amon, C.H., 1997, "Oscillatory Momentum Transport Mechanisms in Transitional Complex Geometry Flows," Journal of Fluids Engineering, Vol. 119, pp. 1-7.

Patera, A.T., 1984, "A Spectral Element Method for Fluid Dynamics: Laminar Flow in a Channel Expansion," Journal of Computational Physics, Vol. 54, No. 3, pp. 468-488.

Rojas, L.R., and Amon, C.H., 1995, "Direct Numerical Simulations of Boundary Layer Instabilities in Subsonic Cascade Flows Triggered by Free-Stream Disturbances," Proceedings of the Third Caribbean Congress on Fluid Dynamics and the Third Latin-American Symposium on Fluid Mechanics, Caracas, Venezuela.

Rojas, L.R., and Amon, C.H., 1997, "Resonant Interaction Between Boundary Layer Instabilities and Free-Stream Disturbances in Cascade Flows," to be submitted to Journal of Fluids Engineering.
Rønquist, E., 1988, "Optimal Spectral Element Methods for the Unsteady Three-Dimensional Incompressible Navier-Stokes Equations," PhD. Thesis, Massachusetts Institute of Technology.

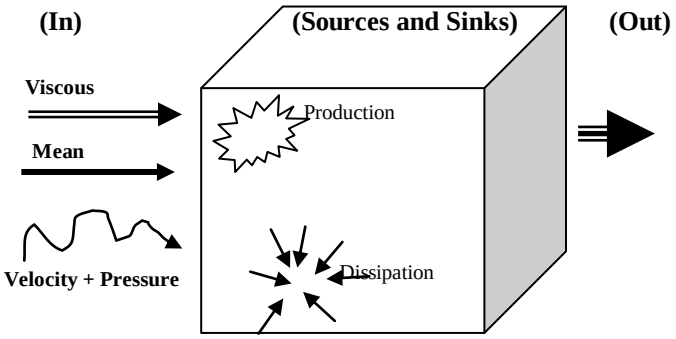

Fig 1 Balance of FKE in elementary control volume

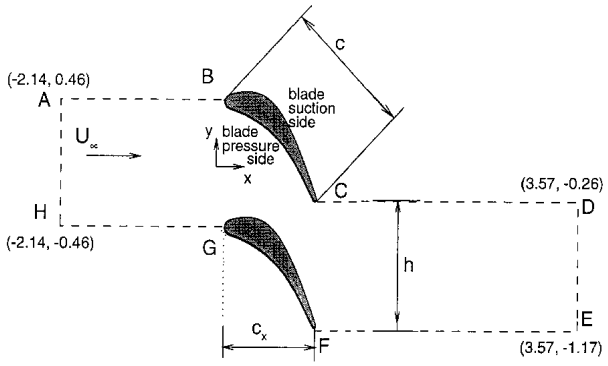

Fig. 2 Two-dimensional computational domain

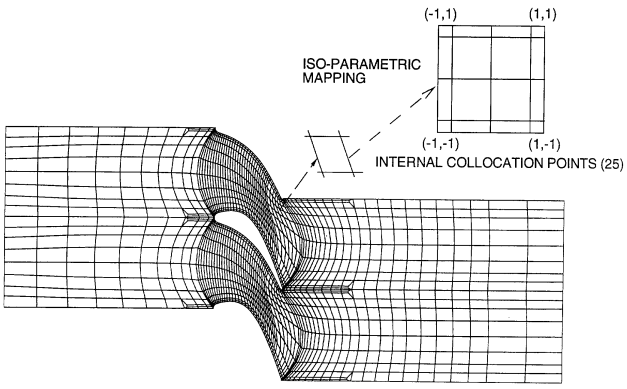

Fig. 3 Mesh discretization. 784 macro-elements

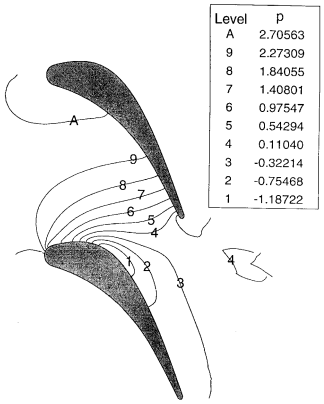

Fig. 4 Mean pressure plot for basic flow at Re=1000

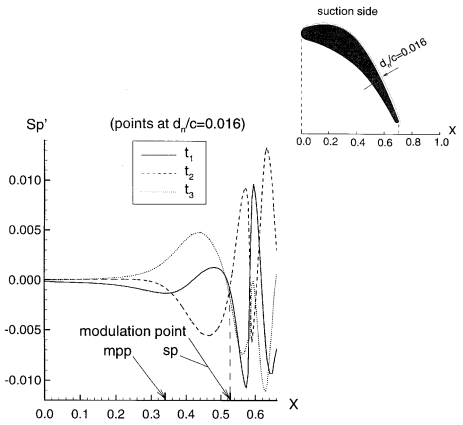

Fig. 5 Wavelength modulation (generation of T-S wave). Sp' vs. X, time for basic flow at Re=1000

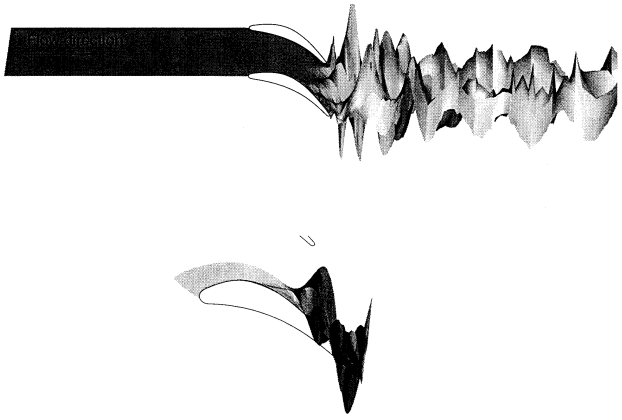

Fig. 6 Carpet plot of Sp'at a characteristic time for basic flow at Re=1000

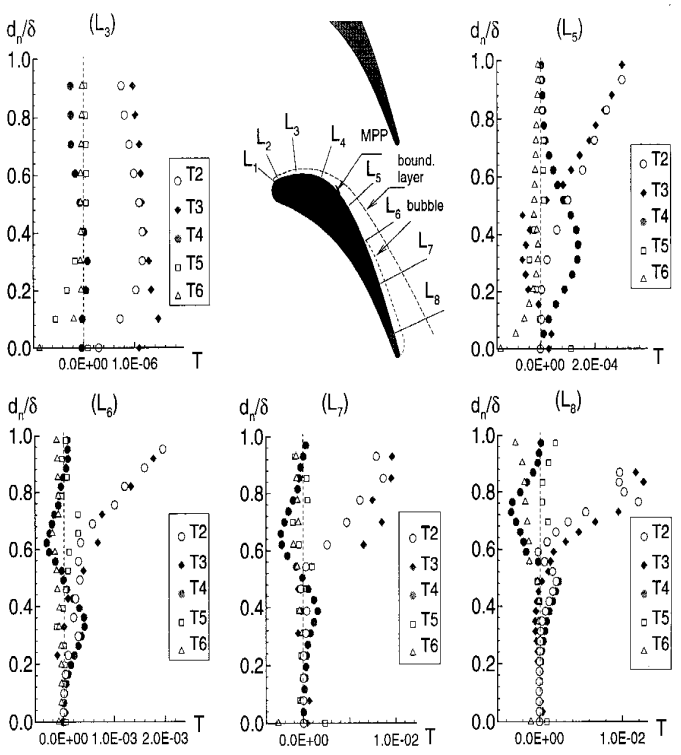

Fig. 7 FKE budget across boundary layer perpendicular stations. basic flow at Re=1000

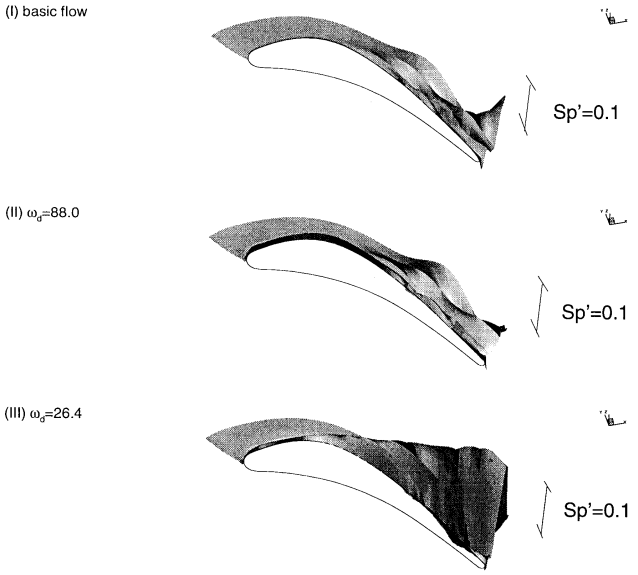

Fig. 8 Sp'at the moment when inlet perturbation vanishes for supercritical perturbed flow for Re=1000, ε=0.02, (a) Basic flow; (b) ω_d=88.0; (c) ω_d=26.4

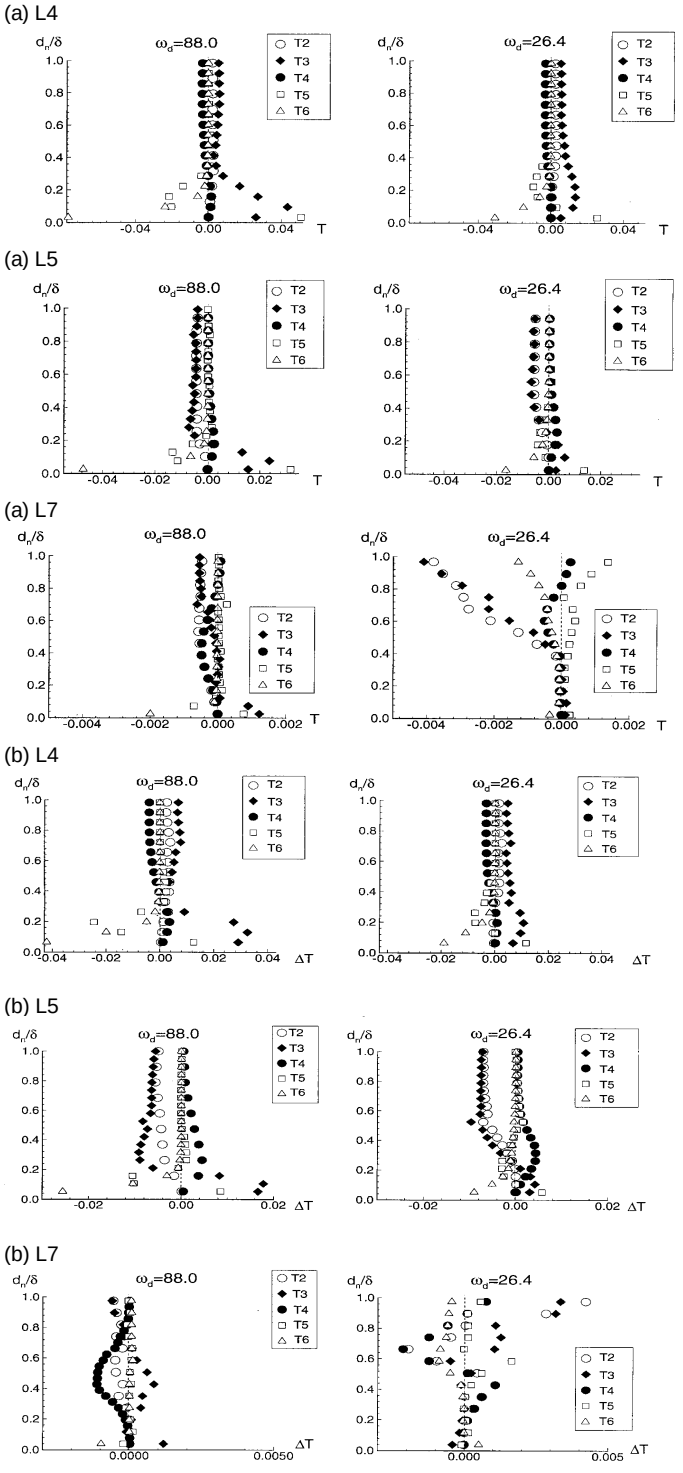

Fig. 9 Changes in FKE terms across the boundary layer for perturbed flows with ε=0.02 and ω_d=88.0 and ω_d=26.4. (a) Re=231; (b) Re=1000